

Article

# New As-Rich Arsenato-Polyoxovanadate Clusters: Solvothermal Synthesis and Selected Properties of $[V_6^{IV}As_8^{III}O_{26}]^{4-}$ Cluster-Containing Compounds

Maren Rasmussen, Christian Näther and Wolfgang Bensch \* 

Institute for Inorganic Chemistry, Kiel University, Max-Eyth-Str. 2, D-24118 Kiel, Germany

\* Correspondence: wbensch@ac.uni-kiel.de

**Abstract:** Three new arsenato-polyoxovanadates with the composition  $[M(en)_3]_2[V_6As_8O_{26}]$  ( $M = Co^{2+}$  (I),  $Zn^{2+}$  (II), and  $Cd^{2+}$  (III)) were synthesized under solvothermal conditions in high yields, thus significantly enhancing the knowledge of As-rich polyoxovanadate cluster chemistry. The compounds are isostructural and feature the very rare  $[V_6^{IV}As_8^{III}O_{26}]^{4-}$  cluster anion. The cluster shell is constructed by interconnection of two trimeric  $\{V_3O_{11}\}$  groups consisting of three edge-sharing  $VO_5$  polyhedra and four  $As_2O_5$  units, which are formed by two corner-sharing  $AsO_3$  pyramids. While the  $As_2O_5$  group is a common structural feature in arsenato-polyoxovanadates, the  $\{V_3O_{11}\}$  unit is only observed in V-rich high-nuclear heteroatom-containing polyoxovanadates  $\{V_{14}E_8\}$  ( $E = As, Sb, Ge$ ). The complexes adopt the  $\Lambda$  ( $\delta\delta\delta$ ) conformation, which is the most stable arrangement. Interestingly, the unit cell parameters do not scale with the volume of the  $[M(en)_3]^{2+}$  complexes, assuming a constant volume of the anion. Only a very detailed Hirshfeld surface analysis revealed that the van der Waals volume of the  $\{V_6As_8O_{26}\}$  moiety is the smallest for the Cd-containing compound, while the volumes of the anions in the other two compounds are very similar. Therefore, the observed trends of the lattice parameters can be explained on the basis of these findings. Furthermore, intermolecular interactions include  $As \cdots H$  contacts in addition to  $O \cdots H$  and  $H \cdots H$  interactions. The electronic spectrum of I contains d–d transitions of the vanadyl group and of the  $Co^{2+}$  cation. As expected only the d–d transitions of the  $VO^{2+}$  unit occur for II and III.

**Keywords:** arsenato-polyoxovanadates; solvothermal synthesis; crystal structures; Hirshfeld surface analysis; spectroscopic properties



**Citation:** Rasmussen, M.; Näther, C.; Bensch, W. New As-Rich Arsenato-Polyoxovanadate Clusters: Solvothermal Synthesis and Selected Properties of  $[V_6^{IV}As_8^{III}O_{26}]^{4-}$  Cluster-Containing Compounds. *Crystals* **2022**, *12*, 1473. <https://doi.org/10.3390/cryst12101473>

Academic Editor: Witold Łojkowski

Received: 16 September 2022

Accepted: 14 October 2022

Published: 18 October 2022

**Publisher's Note:** MDPI stays neutral with regard to jurisdictional claims in published maps and institutional affiliations.



**Copyright:** © 2022 by the authors. Licensee MDPI, Basel, Switzerland. This article is an open access article distributed under the terms and conditions of the Creative Commons Attribution (CC BY) license (<https://creativecommons.org/licenses/by/4.0/>).

## 1. Introduction

The synthesis and characterization of polyoxometalates (POMs) with the elements V, Mo and W [1–6] is a still growing research field because several POMs show promising properties for applications in technologically important areas such as catalysis [7–12], in biomedicine [13–15], sorption of molecules [16] or in molecular electronics [17]. The most commonly applied synthesis methods are reactions at room or at moderate temperatures (reflux) in polar media such as water applying small molecular moieties which form larger cluster anions by self-assembly and condensation reactions [18]. However, many compounds were also synthesized using large, preformed POMs and/or applying hydrothermal conditions. It needs to be mentioned that not only artificial POMs are known, but a large number of POMs were also found in minerals [19], with several of them having no counterpart in synthetically produced compounds.

Among the main group element containing polyoxovanadates (POVs) the first cluster with integrated As (III) cations (As-POV),  $[V_{15}As_6O_{42}(H_2O)]^{6-}$ , was already reported in 1988 [20]. The spherical cluster shell contains fifteen  $VO_5$  pyramids and three  $As_2O_5$  handles. The cavity of the shell hosts a water molecule. The V centers are in the oxidation state +4 and the compound contains 15 unpaired electrons leading to highly

interesting and unusual magnetic properties. Hence, this cluster was intensively investigated in the past and more than 60 papers were published [21]. The chemistry of As-POVs and other heteroatom-containing POVs was systematically developed during the last decades with the main aims to enrich the structure varieties and to alter the physical properties [20]. A large variety of As-POVs exhibiting different geometries and different V:As ratios were reported and selected examples are  $[V_{10}AsO_{26}(H_2O)]$  [22],  $K_7[V_{14}AsO_{40}]$  [23],  $K_3[V_{12}As_3O_{42}]$  [24],  $[Ln(H_2O)_6]_2V_{14}As_8O_{42}(SO_3)$  ( $Ln = La^{3+}$ ,  $Sm^{3+}$ , and  $Ce^{3+}$ ) [25],  $(NH_4)_4[V_{12}As_8O_{40}(H_2O)]$  [26],  $[Cd(dien)]_2[Cd(dien)(H_2O)]_2[V_{16}As_4O_{42}(H_2O)]$ , [27]. The crystal structure of the most As-rich As-POV,  $[V_6As_8O_{26}]^{4-}$ , features two trimeric units  $\{V_3O_{11}\}$  which are joined by four  $As_2O_5$  handles formed by  $AsO_3$  pyramids sharing a common oxygen atom [28]. The compound was prepared under ambient conditions and no further compounds with this anion were reported until recently. This is a surprising observation because dozens of As-POVs were reported during the last decades. Interestingly, most of these compounds were synthesized under solvothermal conditions and all of them contain V-rich high nuclear clusters. One possible explanation that the As-rich cluster was not obtained in solvothermal syntheses may be a low stability under these special conditions. By systematic variation of the solvothermal reaction parameters we were able to synthesize  $[Ni(en)_3]_2[V_6As_8O_{26}]$  ( $en = ethylenediamine$ ) [29] which represents the second structure comprising the  $[V_6^{IV}As_8^{III}O_{26}]^{4-}$  cluster. Solvothermal reactions are complex, and prediction of the reaction product is very limited. Nevertheless, to enhance the knowledge of As-rich POVs further explorative solvothermal syntheses were performed and we were able to prepare three compounds containing the rare  $[V_6^{IV}As_8^{III}O_{26}]^{4-}$  cluster anion, namely  $[M(en)_3]_2[V_6As_8O_{26}]$  ( $M = Co^{2+}$  (I),  $Zn^{2+}$  (II), and  $Cd^{2+}$  (III)). Here, we report on the syntheses, crystal structures and selected properties of these three compounds.

## 2. Materials and Methods

### 2.1. Reagents for the Syntheses of $[M(en)_3]_2[V_6As_8O_{26}]$ ( $M = Co, Zn, and Cd$ )

The chemicals were used as purchased:  $NH_4VO_3$  (Merck PA, 99%);  $As_2O_3$  (Merck PA, 99.5%);  $Zn(CH_3COO)_2 \cdot 2H_2O$  (Merck 99%);  $CoCl_2 \cdot 6H_2O$  (VWR 98%);  $CdCl_2 \cdot 2.5H_2O$  (Sigma Aldrich, Singapore, 99.995%).

### 2.2. Syntheses

All syntheses were performed in glass tubes (volume: 11 mL), heating the reaction mixtures at 150 °C for up to 4 d. Subsequently, the glass tubes were cooled down and the solids were filtered off. In all syntheses a green product was obtained containing needle-like crystals suitable for single crystal structure determination. The products were washed with water and ethanol and were stored in a desiccator. Upscaling experiments were performed in steel autoclaves with a 30 mL Teflon liner. The temperature of 150 °C was held for 4 d followed by cooling the autoclave to room temperature. The treatment of the reaction products was identical with that obtained in glass tubes.

For all syntheses in glass tubes, 1.341 mmol  $NH_4VO_3$  (156.9 mg) and 1.194 mmol  $As_2O_3$  (236.2 mg) were used. For I, 0.66 mmol (157 mg)  $CoCl_2 \cdot 6H_2O$ ; for II, 0.66 mmol (145 mg)  $Zn(CH_3COO)_2 \cdot 2H_2O$ ; and for III, 0.66 mmol (150.8 mg)  $CdCl_2 \cdot 2.5H_2O$  were mixed with the other solid educts. The liquid was composed of 1.7 mL ethylenediamine, and 2.3 mL  $H_2O$  was added to the solid and the slurry was shaken. The syntheses in the autoclaves were performed using a quadrupled amount of solids and liquid. The yields based on  $NH_4VO_3$  were 65% for I, 58% for II and 90% for III.

### 2.3. X-ray Powder Diffraction

The X-ray powder diffraction patterns were collected with a STOE Stadi-P diffractometer using a MYTHEN 1K detector (DECTRIS) and monochromatized  $Cu-K_{\alpha 1}$  radiation ( $\lambda = 1.540598 \text{ \AA}$ ). The experimental and the calculated patterns match perfectly indicating phase purity of the samples (Figure S1).

#### 2.4. Spectroscopic Characterization and Chemical Composition

The infrared spectra were recorded at 295 K with a Bruker Vertex70 FT-IR spectrometer.

The UV/vis diffuse reflectance spectra were measured using the UV/vis two-channel spectrometer Cary 5 from Carian Techtron Pty., Darmstadt and BaSO<sub>4</sub> served as white standard. The raw data were converted into the Kubelka–Munk factor.

Energy dispersive X-ray analysis (EDX) on selected single crystals of I–III was performed with an Environmental Scanning Electron Microscope ESEM XL30 from Philips. I: Co:V:As = 1:5.97:8.04; II: Zn:V:As = 1:6.05:7.94; III: Cd:V:As = 1:6.06:8.05.

#### 2.5. Crystal Structure Determination

Single crystal data collections were performed with a STOE Imaging Plate Diffraction System (IPDS-2) using Cu-K $\alpha$  radiation ( $\lambda = 1.54184 \text{ \AA}$ ). Structure solution was performed with SHELXT [30] and structure refinements were performed against F<sub>2</sub> using SHELXL-2016 [31]. All non-hydrogen atoms were refined with anisotropic displacement parameters. The C–H and N–H hydrogen atoms were positioned with idealized geometry and were refined isotropically with Uiso (H) = 1.2 Ueq (C) using a riding model. Selected crystal data and refinement results are listed in Table 1.

**Table 1.** Selected crystal data and details of the single crystal structure refinements for I, II, and III.

Compound	I	II	III
formula	C <sub>12</sub> H <sub>48</sub> As <sub>8</sub> Co <sub>2</sub> N <sub>12</sub> O <sub>26</sub> V <sub>6</sub>	C <sub>12</sub> H <sub>48</sub> As <sub>8</sub> N <sub>12</sub> O <sub>26</sub> V <sub>6</sub> Zn <sub>2</sub>	C <sub>12</sub> H <sub>48</sub> As <sub>8</sub> Cd <sub>2</sub> N <sub>12</sub> O <sub>26</sub> V <sub>6</sub>
MW/g mol <sup>−1</sup>	1799.48	1812.36	1906
crystal system	tetragonal	tetragonal	tetragonal
space group	I4 <sub>1</sub> /acd	I4 <sub>1</sub> /acd	I4 <sub>1</sub> /acd
a/Å	20.2849 (5)	20.1813 (3)	19.9293 (3)
b/Å	20.2849 (5)	20.1813 (3)	19.9293 (3)
c/Å	24.4386 (8)	24.5412 (4)	24.8786 (5)
$\alpha$ /°	90	90	90
$\beta$ /°	90	90	90
$\gamma$ /°	90	90	90
V/Å <sup>3</sup>	10,055.9 (6)	9995.3 (3)	9881.2 (4)
T/K	200.0 (1)	200.0 (1)	200.0 (1)
Z	8	8	8
D <sub>calc</sub> /g cm <sup>−3</sup>	2.377	2.409	2.563
$\mu$ /mm <sup>−1</sup>	7.019	7.358	7.333
$\theta_{\max}$ /deg	26.005	26.0005	27.005
measured refl.	24684	31020	37145
R <sub>int</sub>	0.0677	0.0328	0.0486
unique refl.	2482	2455	2687
refl. F <sub>0</sub> > 4 $\sigma$ (F <sub>0</sub> )	2208	2366	2563
parameter	151	152	152
R <sub>1</sub> [F <sub>0</sub> > 4 $\sigma$ (F <sub>0</sub> )]	0.0464	0.0269	0.0486
wR <sub>2</sub> [all data]	0.1079	0.0727	0.1304
GOF	1.144	1.160	1.159
$\Delta\rho_{\max/\min}$ /e Å <sup>−3</sup>	0.422/−0.630	0.373/−0.361	0.665/−0.614

CCDC-2194249 (I), CCDC-2194248 (II) and CCDC-2194250 (III) contain the supplementary crystallographic data for this paper. These data can be obtained free of charge from the Cambridge Crystallographic Data Centre via [https://www.ccdc.cam.ac.uk/data\\_request/cif](https://www.ccdc.cam.ac.uk/data_request/cif) (accessed on 15 September 2022).

### 3. Results and Discussion

#### 3.1. Crystal Structure of I, II and III

The compounds  $[M(en)_3]_2[V_6As_8O_{26}]$  ( $M = Co^{2+}$ ,  $Zn^{2+}$ , and  $Cd^{2+}$ ) are isostructural and crystallize in the tetragonal space group  $I4_1/acd$  with  $Z = 8$ . The lattice parameters (Table 1) do not vary in a regular way and the shortest  $A$  axis and longest  $C$  axis are observed for  $M = Cd^{2+}$ , and most probably the reason for this observation are the differing volumes of the cations and anions (see below). The two unique As atoms are located at general positions, while one independent V atom is on a special position and the second on a general position. Six of the seven unique oxygen atoms are also at general positions and the seventh as well as the  $M^{2+}$  cations are at special positions. All C, N, and H atoms of the  $[M(en)_3]^{2+}$  complexes are at general positions. The  $M^{2+}$  cations are in an octahedral environment of six N donor atoms of three en ligands (Figure S2). The complexes adopt the  $\Lambda$  configuration and the C-C bonds are nearly parallel to the  $C_3$  axis of the molecules, i.e., the en ligands are in the  $\delta$  conformation leading to  $\Lambda(\delta\delta\delta)$  [32], which is the most stable conformation. The  $M^{2+}$ -N bond lengths follow the ionic radii of the cations with the shortest for Co-N (average: 2.170 Å, Supplementary Materials, Table S1), slightly longer bonds for Zn-N (average: 2.190 Å, Table S1) and the longest bonds for Cd-N (average: 2.365 Å, Supplementary Materials, Table S1). The N- $M^{2+}$ -N angles clearly deviate from the ideal values of an octahedron and the three complexes exhibit different degrees of distortion (Supplementary Materials, Table S1). Using the minimum bounding ellipsoid (MBE) approach [33] the volumes of the polyhedra and the distortion expressed by the shape parameter  $S$  were calculated. The smallest volumes are obtained for the  $Co^{2+}$  and  $Zn^{2+}$  centered complexes (42.64 and 43.85 Å<sup>3</sup>) and the largest one for the Cd-containing moiety (55.06 Å<sup>3</sup>). The  $[Co(en)_3]^{2+}$  and  $[Zn(en)_3]^{2+}$  complexes are axially compressed, while  $[Cd(en)_3]^{2+}$  is axially stretched. The  $MN_2C_2$  chelate rings show the gauche conformation. The rings are puckered, and the degree of puckering can be expressed by the N-C-C-N torsion angles of 51.52 and 56.96° for I, 51.08 and 56.34° for II, and 45.00 and 52.60° for III, which all deviate from the expected value of approximately 60° and the deviation is most remarkable for the  $[Cd(en)_3]^{2+}$  complex. Overall, the geometric parameters of the three tris(ethylenediamine) complexes match well with data published in the literature [34,35].

The  $V^{4+}$  cations are in a rectangular pyramidal environment (Figure 1),  $VO_5$ , with the bonding pattern found in POVs: one short  $V = O^{2+}$  bond to the apical O atom (I: 1.600–1.605 Å; II: 1.602–1.606; III: 1.603–1.612 Å) and four longer bonds (I: 1.962–2.001 Å; II: 1.920–2.001 Å; III: 1.932–2.004 Å). The O-V-O angles (Supplementary Materials, Tables S2–S4) clearly show that the  $VO_5$  pyramids are distorted. Applying the MBE approach, the volumes of the polyhedra and the shape parameter  $S$  were calculated (Table 2). Only small differences can be seen demonstrating the rigidity of the  $VO_5$  polyhedra. In all three compounds, the V1 centered polyhedron is axially compressed and that containing V2 is slightly axially stretched.

**Table 2.** Volumes of the  $VO_5$  polyhedra (Å<sup>3</sup>) and of the shape parameter  $S$  using the MBE method.

	Co	Zn	Cd
V1	26.98	26.99	27.12
V2	26.89	27.03	27.04
S (V1)	−0.12	−0.11	−0.12
S (V2)	0.043	0.046	0.037

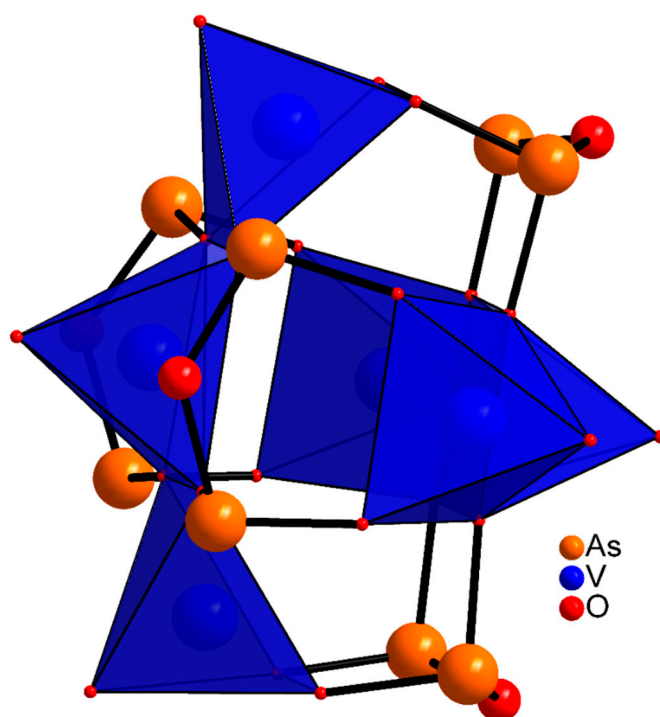


**Figure 1.** Polyhedral representation of the cluster anion  $[V_6As_8O_{26}]^{4-}$  in the structures of the title compound.

The As atoms are in a trigonal–pyramidal environment with average As–O bond lengths of 1.769 (Co), 1.772 (Zn) and 1.773 Å (Cd) (Supplementary Materials, Tables S2–S4). Neighboring  $AsO_3$  pyramids share a common O atom to form four  $As_2O_5$  handle-like moieties (Figure 1). The angles As–O–As are 127.3, 126.8, and 126.6° for M = Co, Zn, and Cd (Supplementary Materials, Tables S2–S4), and agree with those reported earlier [28,29]. Normally, this angle is larger in high-nuclear As-POVs and is in the range from 132 to 136°, indicating that the As–O–As angle is slightly strained.

The cluster  $[V_6As_8O_{26}]^{4-}$  is composed of two symmetry-related trimeric units,  $\{V_3O_{11}\}$ , comprising three  $VO_5$  pyramids sharing common edges (Figure 1). The two  $\{V_3O_{11}\}$  moieties are bridged by the  $As_2O_5$  groups to form the cluster anion, which contains a cavity with dimensions  $4.4 \cdot 7 \text{ \AA}^2$  (measured from coordinate-to-coordinate). The size of the cavity is too small for hosting a guest molecule as is often observed for the larger As-POV cluster anions. All geometric parameters are in good agreement with those published for compounds with the  $[V_6As_8O_{26}]^{4-}$  cluster shell [28,29].

We note that the  $\{V_3O_{11}\}$  building unit is a common motif in high-nuclear heteroatom-containing POVs  $\{V_{14}E_8\}$  (E = As, Sb, Ge) [36–44]. In the crystal structures of these compounds eight edge-sharing  $VO_5$  pyramids form a central ring which is capped on both sides by the  $\{V_3O_{11}\}$  groups, which are rotated by approximately 90° against each other. Removal of the central ring leads to the structure of the cluster anion in the title compounds. Using the bond valence sum (BVS) method, the valence states of V and As were calculated yielding +4 for the V centers and +3 for the As atoms justifying the formula  $[V_6^{IV}As_8^{III}O_{26}]^{4-}$ .

The arrangement of the cations and anions in the structures is shown in Figure 2. The anions form rods along the c-axis and the  $[M(en)_3]^{2+}$  complexes are located in the spaces between the anions in a pairwise manner along  $[1\ 0\ 0]$  and  $[0\ 1\ 0]$  with  $M \cdots M$  separations of  $\approx 7.6 \text{ \AA}$  within the ‘pairs’ and 13.5 Å between the ‘pairs’ (distances are measured from coordinate-to-coordinate).

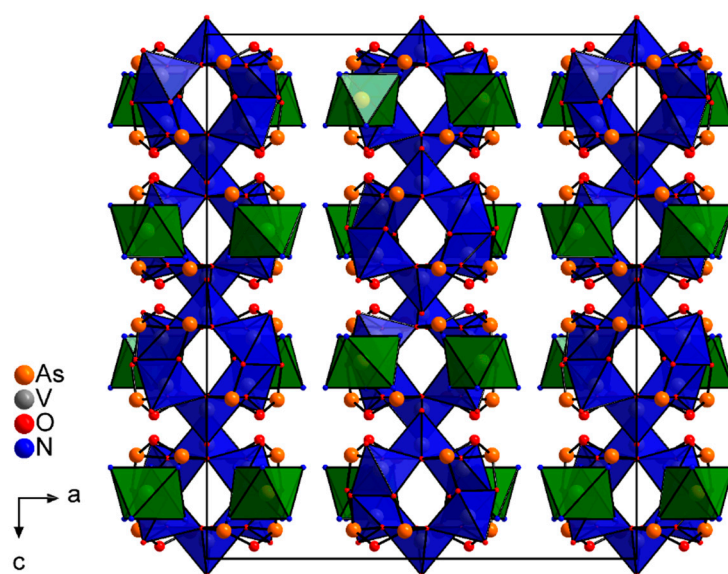


**Figure 2.** View of the arrangement of the constituents in the structure of the title compounds. C and H atoms are omitted for clarity.

### 3.2. Hirshfeld Surface Analysis

Cations and anions are connected by N-H···O and C-H···O hydrogen bonding interactions (Supplementary Materials, Tables S5–S7) generating a three-dimensional network. For gaining more insight into the intermolecular interactions a Hirshfeld surface analysis was performed [45–48]. A Hirshfeld surface is constructed applying the equation

$$d_{norm} = \frac{d_i - r_i^{vdW}}{r_i^{vdW}} + \frac{d_e - r_e^{vdW}}{r_e^{vdW}} \quad (1)$$

$vdW$  = van der Waals radius;  $d_i$  represents the distance of a point on the surface to the nearest nucleus inside the surface;  $d_e$  is the distance from such a point to the next neighbor outside the surface. If an interatomic distance is shorter than the sum of the van der Waals radii, a red area occurs on the Hirshfeld surface, and all other colored regions indicate interatomic distances longer than the sum of the van der Waals radii. The analysis reveals that the differences between the three compounds are relatively small and the Hirshfeld surfaces of the anions and cations for the compounds are shown in Figure 3.

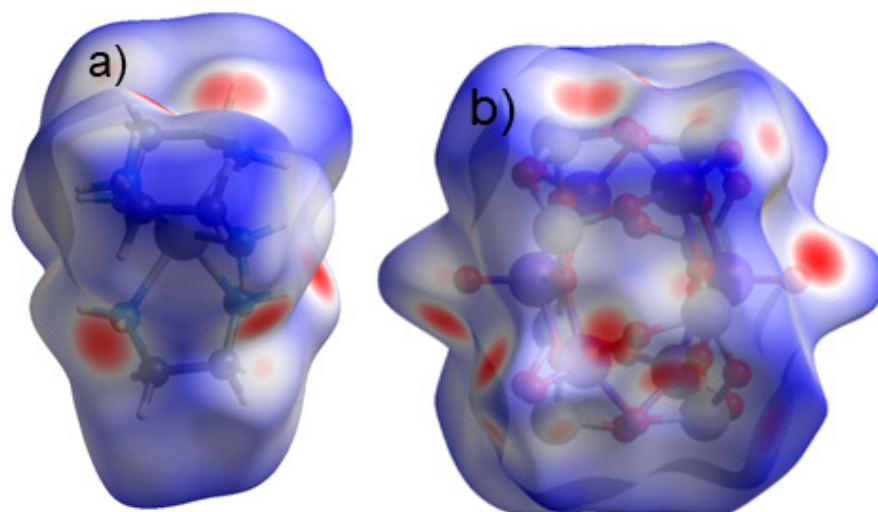


**Figure 3.** Cont.

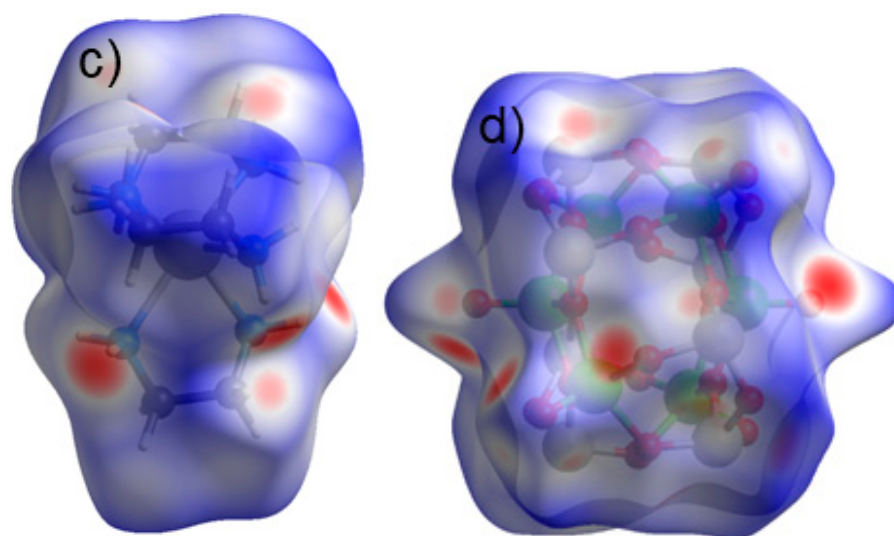


**Figure 3.** The Hirshfeld surfaces of the cation (a) and anion (b) of  $[M(en)_3]_2[V_6As_8O_{16}]$  ( $M = Co, Zn$ ); the Hirshfeld surfaces of the cation (c) and anion (d) of  $[Cd(en)_3]_2[V_6As_8O_{26}]$ . Red areas on the Hirshfeld surface indicate intermolecular distances shorter than the sum of the van der Waals radii.

All the red areas on the Hirshfeld surfaces are caused by intermolecular  $O \cdots H$  interactions to  $NH_2/CH_2$  groups of the en ligands (see also Supplementary Materials, Tables S5–S7 for the geometric parameters of the hydrogen bonds). A further interpretation of the 3D Hirshfeld surface is not straightforward; therefore, a fingerprint plot can be constructed representing a 2D view of the 3D surface (Figure 4). Three different intermolecular interactions are identified for the cations:  $H \cdots H$  (30.3 (Co, Zn) and 33.4% (Cd)),  $H \cdots O$  (54.8 (Co, Zn) and 52.3% (Cd)) and  $H \cdots As$  (15 (Co, Zn) and 14.4% (Cd)). Comparing the fingerprint plots of  $[M(en)_3]^{2+}$  complexes ( $M = Co, Zn$ ) with that of  $[Cd(en)_3]^{2+}$  the sharp spike caused by  $H \cdots O$  interactions appears at the same  $d_e-d_i$  position, but a second less sharp feature occurs for the Cd-containing complex at somewhat longer  $d_e-d_i$  values caused by  $H \cdots H$  interactions, which are located at even longer  $d_e-d_i$  values in the Zn- resp. Co-containing complexes. For the anions the interactions are 74.4% for  $O \cdots H$  and 26.6% for  $As \cdots H$ , and they are virtually identical for the three compounds. For  $As \cdots H$  interactions the shortest contact is at 2.77 (Co), 2.76 (Zn) and 2.85 Å (Cd), which are shorter than the sum of van der Waals radii of 2.95 Å [49]. The corresponding angles  $N-H \cdots As$  are 153.4 (Co), 155 (Zn) and 160.3° (Cd) pointing towards significant interactions. A second  $As \cdots H$  separation at 2.91 (Co), 2.89 (Zn) and 2.87 Å (Cd) with the  $C-H \cdots As$  angles of 156.5 (Co), 154.6 (Zn) and 145.5° (Cd) indicates weaker intermolecular interactions.

The Hirshfeld surface calculations yield further quantities, such as the volumes and areas of the cations and anions. The volumes of the cations do not differ much: 290.87 for I, 289.28 for II and 290.73 Å<sup>3</sup> for III. However, for the anions clearly different volumes were calculated: 649.05 for I, 644.97 for II and 628.89 Å<sup>3</sup> for III. These differences may account for the non-regular changes of the lattice parameters across the series of compounds.

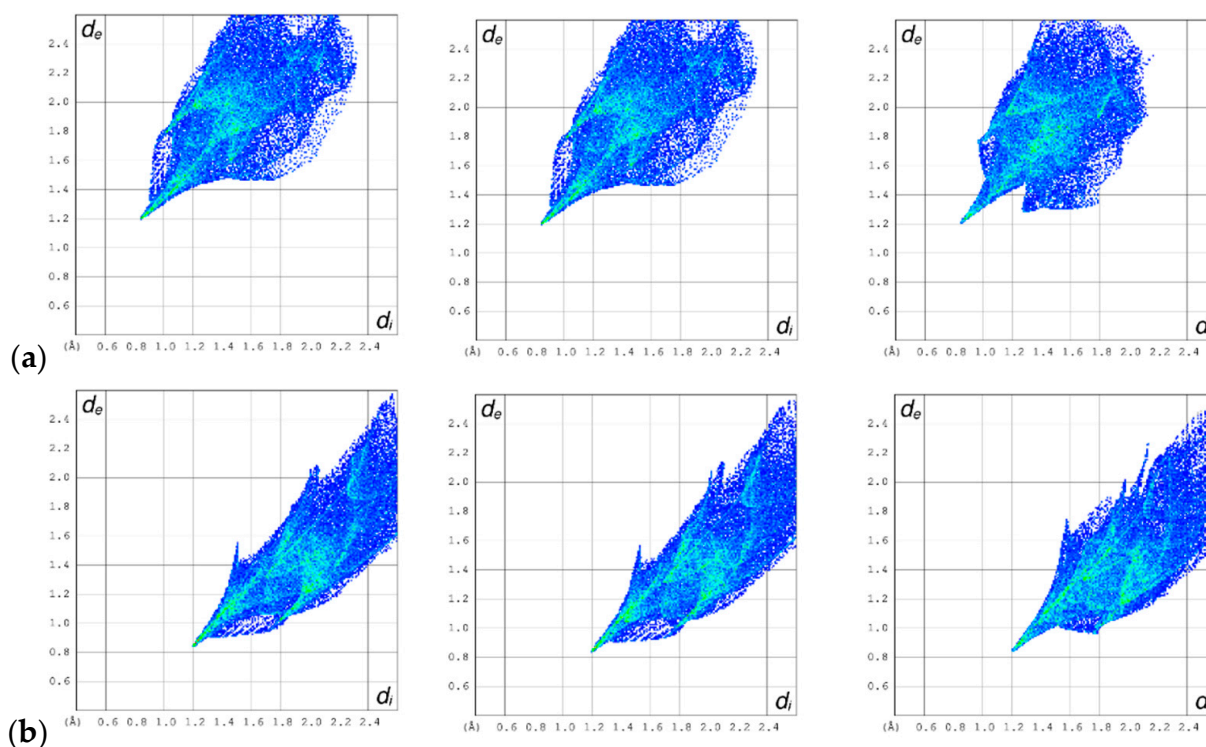


**Figure 4.** (a) the fingerprint plots of the cations in I, II, and III from left to right; (b) fingerprint plots of the anions in I, II, and III in the same order as the cations.

### 3.3. Spectroscopic Investigations

The IR spectra of the three compounds in the fingerprint region are displayed in Figure 5. In the  $\text{NH}_2$  and  $\text{CH}_2$  regions (not shown here) all spectra contain absorptions of the asymmetric and symmetric N-H stretching vibrations:  $3330$ ,  $3309$  and  $3286\text{ cm}^{-1}$  for I,  $3340$ ,  $3315$  and  $3292\text{ cm}^{-1}$  for II, and  $3353$ ,  $3331$  and  $3288\text{ cm}^{-1}$  for III. The bands of the  $\text{CH}_2$  groups are at  $2967$ ,  $2930$ , and  $2885\text{ cm}^{-1}$  for I, at  $2969$ ,  $2931$  and  $2887\text{ cm}^{-1}$  for II, and at  $2969$ ,  $2924$ , and  $2879\text{ cm}^{-1}$  for III. The occurrence of three bands in the N-H region is a typical sign for  $\text{NH}_2$  groups involved in hydrogen bonding interactions. All these signals observed for the title compounds are in agreement with literature values of tris(ethylenediamine) complexes of the cations in I–III [50,51]. The  $\text{NH}_2$  bending vibration occurs at  $1593\text{ cm}^{-1}$  for III, and is split into two signals for I and II ( $1600$  and  $1580\text{ cm}^{-1}$ ). The  $\text{CH}_2$  scissor vibration is located at around  $1465\text{ cm}^{-1}$  and the  $\text{CH}_2$  twist occurs at  $\approx 1330\text{ cm}^{-1}$  for I–III. The strong absorption at  $\approx 960\text{ cm}^{-1}$  is caused by the V=O stretching vibration and is typical for the  $\text{VO}^{2+}$  vanadyl group. For the N-C-C-N skeleton six modes are expected which can be classified as three skeleton stretching vibrations, two N-C-C-N deformation modes and one torsional vibration around the C-C bond. The three stretching bands are between  $900$  and  $1100\text{ cm}^{-1}$ , but the overlap with other absorptions makes a distinct assignment impossible. The remaining absorptions of the skeleton are located at much lower wavenumber around  $500\text{ cm}^{-1}$ . Below  $900\text{ cm}^{-1}$  the V-O-V, V-O-As, As-O-As, and As-O vibrations are located which cannot be unambiguously assigned. According to data in the literature, the M-N stretching modes are clearly located below  $450\text{ cm}^{-1}$ .

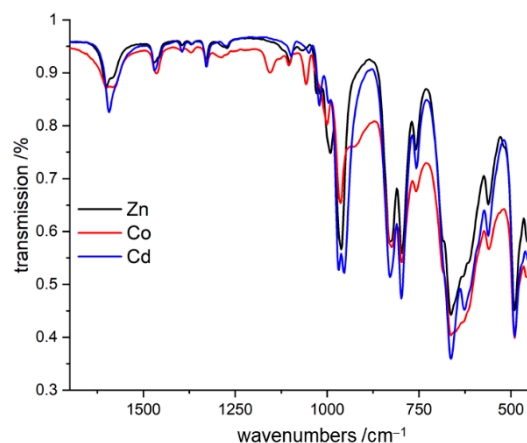


**Figure 5.** The IR spectra of the title compounds in the fingerprint region.

In the UV/vis spectra of the compounds (Figure 6), two absorptions are observed for II and III, which are located at  $\approx 1.5$  ( $12,098 \text{ cm}^{-1}$ ,  $827 \text{ nm}$ ) and  $\approx 2.0 \text{ eV}$  ( $16,131 \text{ cm}^{-1}$ ,  $620 \text{ nm}$ ), while for I an additional signal is present at  $\approx 2.65 \text{ eV}$  ( $21,374 \text{ cm}^{-1}$ ,  $468 \text{ nm}$ ) and the first transition is broader than for II and III. In addition, the absorption maximum of the first signal of I is slightly shifted to lower energy ( $1.44 \text{ eV}$ ,  $11,614 \text{ cm}^{-1}$ ,  $861 \text{ nm}$ ). For compounds II and III, no d–d transitions are possible for the  $d^{10}$  electronic configuration; therefore, the absorptions must be caused by the vanadyl groups. For this group the d–d transitions  ${}^2B_{2g} \rightarrow {}^2E_g$ ,  ${}^2B_{2g} \rightarrow {}^2B_{1g}$  and  ${}^2B_{2g} \rightarrow {}^2A_{1g}$  are expected [52]. Depending on the environment, i.e., packing in the structure, and on the actual distortion of the  $\text{VO}_5$  pyramids, the ideal  $C_{4v}$  symmetry is reduced, and the degeneracy of the first band is removed. This effect may be the reason that the absorption at  $\approx 1.5$  is relatively broad and consists of two overlapping bands. For I the situation is different because for the  $\text{Co}^{2+}$  cation the first d–d transition  ${}^4T_{1g}(F) \rightarrow {}^4T_{2g}(F)$  occurs in the energetic region of the first absorption band of the vanadyl unit and this a further reason for the broadness of the first absorption band in the spectrum of I. The signal at  $\approx 2.65 \text{ eV}$  can be assigned to the  ${}^4T_{1g}(F) \rightarrow {}^4A_{2g}(F)$  transition of the  $\text{Co}^{2+}$  cation. The strong increase in the absorptions above  $3 \text{ eV}$  is most probable caused by charge-transfer processes.

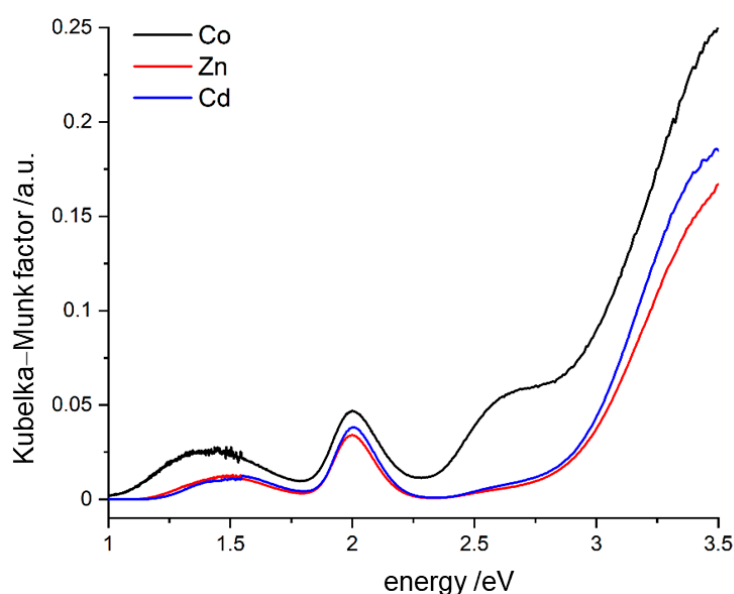


**Figure 6.** The UV/vis spectra of compounds I–III.

#### 4. Conclusions

In this manuscript, we have reported the solvothermal synthesis and selected properties of three new As-rich polyoxovanadates with composition  $[M(en)_3]_2[V_6As_8O_{26}]$  ( $M = Co, Zn, Cd$ ), a significant step forward in the chemistry of As-rich POV clusters. It is surprising that the number of compounds featuring this small As-POV cluster is comparatively low compared with other high-nuclearity As-POVs, especially keeping in mind that the primary building units such as the  $As_2O_5$  handle and the trimeric  $\{V_3O_{11}\}$  group frequently occur in the structures of other As-POVs. From a synthetic point of view, the occurrence of three isostructural compounds prepared under solvothermal conditions is surprising because, in most cases, synthesis recipes cannot be directly transferred from, e.g., one transition metal cation to another. While the overall structural features of the three isostructural compounds are very similar, the Hirshfeld surface analysis reveals some subtle differences in the intermolecular interactions between I/II and III. The analysis identified the reason for the non-continuous variation of the lattice parameters, because one would on a first glance expect a steady change with the ionic radii of the cations. Surprisingly, the anion in III has the smallest van der Waals volume, allowing a denser packing of the constituents along  $[1\ 0\ 0]$ .

**Supplementary Materials:** The following are available online at <https://www.mdpi.com/article/10.3390/cryst12101473/s1>, Figure S1: Experimental and calculated X-ray powder patterns of I–III; Figure S2: ORTEP plots of the  $[M(en)_3]^{2+}$  complexes in the structures of I, II, and III with labelling. Table S1. Selected bond lengths (Å) and angles (°) for the  $M^{2+}$  coordination in I, II, and III. Table S2. Selected bond lengths (Å) and angles (°) for the  $[V_6As_8O_{26}]^{4-}$  anion in I. Table S3. Selected bond lengths (Å) and angles (°) for the  $[V_6As_8O_{26}]^{4-}$  anion in II. Table S4. Selected bond lengths (Å) and angles (°) for the  $[V_6As_8O_{26}]^{4-}$  anion in III. Table S5. Hydrogen bonds [Å and °] for I. Table S6. Hydrogen bonds [Å and °] for II. Table S7. Hydrogen bonds [Å and °] for III.

**Author Contributions:** Conceptualization, methodology, funding and writing of draft: W.B.; syntheses and basic characterization: M.R.; single crystal structure determination: C.N. All authors have read and agreed to the published version of the manuscript.

**Funding:** This research received no external funding.

**Institutional Review Board Statement:** Not applicable.

**Informed Consent Statement:** Not applicable.

**Data Availability Statement:** Data are within the article or the supplementary information.

**Acknowledgments:** The authors thank the State of Schleswig-Holstein for financial support.

**Conflicts of Interest:** The authors declare no conflict of interest.

#### References

1. Müller, A.; Kögerler, P. From simple building blocks to structures with increasing size and complexity. *Coord. Chem. Rev.* **1999**, *182*, 3–17. [[CrossRef](#)]
2. Gouzerh, P.; Proust, A.A. Main-group element, organic, and organometallic derivatives of polyoxometalates. *Chem. Rev.* **1998**, *98*, 77–112. [[CrossRef](#)]
3. Pope, M.T.; Müller, A. Polyoxometalate chemistry: An old field with new dimensions in several disciplines. *Angew. Chem. Int. Ed. Engl.* **1991**, *30*, 34–48. [[CrossRef](#)]
4. Monakhov, K.Y.; Bensch, W.; Kögerler, P. Semimetal-functionalised polyoxovanadates. *Chem. Soc. Rev.* **2015**, *44*, 8443–8483. [[CrossRef](#)]
5. Hill, C.L. Introduction: Polyoxometalates - Multicomponent Molecular Vehicles To Probe Fundamental Issues and Practical Problem. *Chem. Rev.* **1998**, *98*, 1–2.
6. Long, D.-L.; Burkholder, E.; Cronin, L. Polyoxometalate clusters, nanostructures and materials: From self-assembly to designer materials and devices. *Chem. Soc. Rev.* **2007**, *36*, 105–121. [[CrossRef](#)]
7. Okuhara, T.; Mizuno, N.; Misono, M. Catalysis by heteropoly compounds—Recent developments. *Appl. Catal. A Gen.* **2001**, *222*, 63–77. [[CrossRef](#)]
8. Kamata, K.; Yonehara, K.; Nakagawa, Y.; Uehara, K.; Mizuno, N. Efficient stereo and regioselective hydroxylation of alkanes catalysed by a bulky polyoxometalate. *Nat. Chem.* **2010**, *2*, 478–483. [[CrossRef](#)]

9. Samaniyan, M.; Mirzaei, M.; Khajavian, R.; Eshtiagh-Hosseini, H.; Streb, C. Heterogeneous catalysis by polyoxometalates in metal—Organic frameworks. *ACS Catal.* **2019**, *9*, 10174–10191. [[CrossRef](#)]
10. Kamata, K.; Sugahara, K. Base catalysis by mono and polyoxometalates. *Catalysts* **2017**, *7*, 345. [[CrossRef](#)]
11. Lian, L.; Zhang, H.; An, S.; Chen, W.; Song, Y.-F. Polyoxometalates-based heterogeneous catalysts in acid catalysis. *Sci. China Ser. B Chem.* **2021**, *64*, 1117–1130. [[CrossRef](#)]
12. Katsoulis, D.E. A survey of applications of polyoxometalates. *Chem. Rev.* **1998**, *98*, 359–388. [[CrossRef](#)]
13. Bijelic, A.; Aureliano, M.; Rompel, A. Polyoxometalates as potential next-generation metallodrugs in the combat against cancer. *Angew. Chem. Int. Ed.* **2019**, *58*, 2980–2999. [[CrossRef](#)]
14. Bijelic, A.; Aureliano, M.; Rompel, A. The antibacterial activity of polyoxometalates: Structures, antibiotic effects and future perspectives. *Chem. Commun.* **2018**, *54*, 1153–1169. [[CrossRef](#)]
15. Qi, W.; Zhang, B.; Qi, Y.; Guo, S.; Tian, R.; Sun, J.; Zhao, M. The Anti-proliferation activity and mechanism of action of  $K_{12}[V_{18}O_{42}(H_2O)] \cdot 6H_2O$  on breast cancer cell lines. *Molecules* **2017**, *22*, 1535. [[CrossRef](#)]
16. Uchida, S.; Mizuno, N. Design and syntheses of nano-structured ionic crystals with selective sorption properties. *Coord. Chem. Rev.* **2007**, *251*, 2537–2546. [[CrossRef](#)]
17. Izarova, N.V.; Kögerler, P. *Trends in Polyoxometalates Research*; Ruhlmann, L., Schaming, D., Eds.; Nova Science Publishers Inc.: New York, NY, USA, 2015.
18. Hutin, M.; Rosnes, M.H.; Long, D.-L.; Cronin, L. *Comprehensive Inorganic Chemistry II*; Reedijk, J., Poeppelmeier, K., Eds.; Elsevier: Oxford, UK, 2013; Volume 2, pp. 2241–2269.
19. Krivovichev, S.V. Polyoxometalate clusters in minerals: Review and complexity analysis. *Acta Crystallogr. Sect. B Struct. Sci. Cryst. Eng. Mater.* **2020**, *76*, 618–629. [[CrossRef](#)]
20. Müller, A.; Döring, J. A novel heterocluster with D<sub>3</sub>-symmetry containing twenty-one core atoms:  $[As_6^{III}V_{15}^{IV}O_{42}(H_2O)]^{6-}$ . *Angew. Chem. Int. Ed. Engl.* **1988**, *27*, 1721. [[CrossRef](#)]
21. Kögerler, P.; Tsukerblat, B.; Müller, A. Structure-related frustrated magnetism of nanosized polyoxometalates: Aesthetics and properties in harmony. *Dalton Trans.* **2009**, *39*, 21–36. [[CrossRef](#)]
22. Bu, W.-M.; Ye, L.; Yang, G.-Y.; Shao, M.-C.; Fan, Y.-G.; Xu, J.-Q. A three-dimensional neutral framework of a novel decavanadium cluster bridged by an  $AsO_4$  tetrahedron:  $[AsV^{IV}_8V^{V}_2O_{26}(\mu-H_2O)] \cdot 8H_2O$ . *Chem. Commun.* **2000**, *14*, 1279–1280. [[CrossRef](#)]
23. Müller, A.; Döring, J.; Khan, M.I.; Wittneben, V.  $[As^{V}V_{12}^{V}V_2^{IV}O_{40}]^{7-}$ , a topologically interesting, mixed valence cluster as model for vanadium minerals formed by weathering. *Angew. Chem. Int. Ed. Engl.* **1991**, *30*, 210–212. [[CrossRef](#)]
24. Khan, M.I.; Chen, Q.; Zubieta, J. Hydrothermal syntheses and structures of reduced and mixed valence polyoxovanadium clusters with capped cage cores:  $K_3[H_{12}(AsO)_2(AsO_4)V_6^{IV}V_6^{V}O_{36}] \cdot 12H_2O$  and  $Rb_5[(As_2O)_4(VO)_2V_{12}^{IV}O_{36}Cl] \cdot 2H_2O$ . *Inorganica Chim. Acta* **1993**, *212*, 199–206. [[CrossRef](#)]
25. Arumuganathan, T.; Das, S.K. Discrete polyoxovanadate cluster into an organic free metal-oxide-based material: Syntheses, crystal structures, and magnetic properties of a new series of lanthanide linked-POV compounds  $\{[Ln(H_2O)_6]_2As_8V_{14}O_{42}(SO_3)\} \times 8H_2O$  (Ln =  $La^{3+}$ ,  $Sm^{3+}$ , and  $Ce^{3+}$ ). *Inorg. Chem.* **2009**, *48*, 496–507. [[CrossRef](#)]
26. Wutkowski, A.; Evers, N.; Bensch, W. Synthesis, structure, and solubility studies of a new arsenato-polyoxovanadate cluster compound:  $(NH_4)_4[V_{12}As_8O_{40}(H_2O)] \cdot 4H_2O$ . *Z. Anorg. Allg. Chem.* **2011**, *637*, 2205–2210. [[CrossRef](#)]
27. Zhou, J.; Zheng, S.-T.; Fang, W.-H.; Yang, G.-Y. A new 2-D network containing  $\{As_4V_{16}O_{42}(H_2O)\}$  cluster units. *Eur. J. Inorg. Chem.* **2009**, *2009*, 5075–5078. [[CrossRef](#)]
28. Dumas, E.; Livage, C.; Sabine Halut, S.; Herve, G. Synthesis and molecular structure of a new arsenic rich polyoxovanadium anion,  $[As_8^{III}V_6^{IV}O_{26}]^{4-}$ . *Chem. Commun.* **1996**, *21*, 2437–2438. [[CrossRef](#)]
29. Kondinski, A.; Rasmussen, M.; Mangelsen, S.; Pienack, N.; Simjanoski, V.; Näther, C.; Stares, D.L.; Schalley, C.A.; Bensch, W. Composition-driven archetype dynamics in polyoxovanadates. *Chem. Sci.* **2022**, *13*, 6397–6412. [[CrossRef](#)]
30. Sheldrick, G.M. SHELXT—Integrated space-group and crystal-structure determination. *Acta Cryst. A* **2015**, *71*, 3–8.
31. Sheldrick, G.M. Crystal structure refinement with SHELXL. *Acta Crystallogr. C* **2015**, *71*, 3–8. [[CrossRef](#)]
32. Beattie, J.K. Conformational analysis of tris(ethylenediamine) complexes. *Accounts Chem. Res.* **1971**, *4*, 253–259. [[CrossRef](#)]
33. Cumby, J.; Atfield, J.P. Ellipsoidal analysis of coordination polyhedra. *Nat. Commun.* **2017**, *8*, 14235. [[CrossRef](#)]
34. Pham, D.N.K.; Roy, M.; Golen, J.A.; Manke, D.R. The first-row transition-metal series of tris(ethylenediamine) diacetate complexes  $[M(en)_3](OAc)_2$  (M is Mn, Fe, Co, Ni, Cu, and Zn). *Acta Cryst. C* **2017**, *73*, 442–446. [[CrossRef](#)]
35. Ma, G.; Fischer, A.; Nieuwendaal, R.; Ramaswamy, K.; Hayes, S.E. Cd(II)–ethylenediamine mono- and bimetallic complexes—Synthesis and characterization by <sup>113</sup>Cd NMR spectroscopy and single crystal X-ray diffraction. *Inorganica Chim. Acta* **2005**, *358*, 3165–3173. [[CrossRef](#)]
36. Huan, G.; Greaney, M.A.; Jacobson, A.J. The synthesis and crystal structure of a new polyoxovanadium cluster anion:  $[As^{III}_8V^{IV}_{14}O_{42}(0.5H_2O)]^{4-}$ . *J. Chem. Soc. Chem. Commun.* **1991**, *4*, 260–261. [[CrossRef](#)]
37. Guo, H.-Y.; Li, Z.-F.; Fu, L.-W.; Hu, Y.-Y.; Cui, X.-B.; Liu, B.-J.; Xu, J.-N.; Huo, Q.-S.; Xu, J.-Q. Structural influences of arsenic-vanadium clusters and transition metal complexes on final structures of arsenic–vanadium-based hybrids. *Inorganica Chim. Acta* **2016**, *443*, 118–125. [[CrossRef](#)]
38. Wang, C.; Zhou, G.; Zhang, Z.; Zhu, D.; Xu, Y. Hydrothermal synthesis, characterization, and luminescence of two new ar-senic-vanadium compounds with a  $\gamma$ - $[As_8V_{14}O_{42}(H_2O)]^{4-}$  anions. *J. Coord. Chem.* **2011**, *64*, 1198–1206. [[CrossRef](#)]

39. Wendt, M.; Näther, C.; van Leusen, J.; Kögerler, P.; Bensch, W. Mixing Sb<sup>III</sup> and Ge<sup>IV</sup> occupancy in the polyoxovanadate {V<sub>14</sub>E<sub>8</sub>} archetype. *Z. Nat. B* **2018**, *73*, 773–779. [[CrossRef](#)]
40. Wendt, M.; Näther, C.; Bensch, W. The high nuclearity antimonato-polyoxovanadate cluster {V<sub>15</sub>Sb<sub>6</sub>O<sub>42</sub>} as synthon for the solvothermal in-situ generation of  $\alpha$ - and  $\beta$ -{V<sub>14</sub>Sb<sub>8</sub>O<sub>42</sub>} isomers. *Chem. Eur. J.* **2016**, *22*, 7747–7751. [[CrossRef](#)]
41. Cui, X.-B.; Xu, J.-Q.; Li, Y.; Sun, Y.-H.; Ye, L.; Yang, G.-Y. Hydrothermal synthesis and characterization of (enH<sub>2</sub>)<sub>3.5</sub>[As<sub>8</sub>V<sub>14</sub>O<sub>42</sub>(PO<sub>4</sub>)]·2H<sub>2</sub>O. *J. Mol. Struct.* **2003**, *657*, 397–403. [[CrossRef](#)]
42. Pitzschke, D.; Wang, J.; Hoffmann, R.-D.; Pöttgen, R.; Bensch, W. Two compounds containing the first mixed Germanium-Vanadium-Polyoxothioanion [V<sub>14</sub>Ge<sub>8</sub>O<sub>42</sub>S<sub>8</sub>]<sup>12-</sup>. *Angew. Chem. Int. Ed.* **2006**, *45*, 1305–1308. [[CrossRef](#)]
43. Qi, Y.; Li, Y.; Wang, E.; Jin, H.; Zhang, Z.; Wang, X.; Chang, S. Syntheses and structures of four organic–inorganic hybrids based on the surface restricted [As<sup>III</sup><sub>8</sub>V<sup>IV</sup><sub>14</sub>O<sub>42</sub>] building unit and various zinc coordination groups. *Inorg. Chim. Acta* **2007**, *360*, 1841–1853. [[CrossRef](#)]
44. Qi, Y.; Li, Y.; Wang, E.; Zhang, Z.; Chang, S. Metal-controlled self-assembly of arsenic—Vanadium-cluster backbones with organic ligands. *Dalton Trans.* **2008**, *17*, 2335–2345. [[CrossRef](#)]
45. Spackman, M.A. Molecules in crystals. *Phys. Scr.* **2013**, *87*, 48103. [[CrossRef](#)]
46. Spackman, M.A.; McKinnon, J.J. Fingerprinting intermolecular interactions in molecular crystals. *Cryst. Eng. Comm.* **2002**, *4*, 378–392. [[CrossRef](#)]
47. Spackman, M.A.; Jayatilaka, D. Hirshfeld surface analysis. *Cryst. Eng. Comm.* **2009**, *11*, 19–32.
48. Spackman, P.R.; Turner, M.J.; McKinnon, J.J.; Wolff, S.K.; Grimwood, D.J.; Jayatilaka, D.; Spackman, M.A. Crystal explorer: A program for Hirshfeld surface analysis, visualization and quantitative analysis of molecular crystals. *J. Appl. Crystallogr.* **2021**, *54*, 1006–1011. [[CrossRef](#)]
49. Mantina, M.; Chamberlin, A.C.; Valero, R.; Cramer, C.J.; Truhlar, D.G. Consistent van der Waals radii for the whole main group. *J. Phys. Chem. A* **2009**, *113*, 5806–5812. [[CrossRef](#)]
50. Bennett, A.M.; Foulds, G.A.; Thornton, D.A. The i.r. spectra of ethylenediamine complexes—I. The tris(ethylenediamine) complexes of first transition series metal(II) sulphates. *Spectrochim. Acta Part A Mol. Spectrosc.* **1989**, *45*, 219–223. [[CrossRef](#)]
51. Krishnan, K.; Plane, R.A. Raman and infrared spectra of complexes of ethylenediamine with Zinc(II), Cadmium(II), and Mercury(II). *Inorg. Chem.* **1966**, *5*, 852–857. [[CrossRef](#)]
52. Ballhausen, C.J.; Gray, H.B. The electronic structure of the vanadyl ion. *Inorg. Chem.* **1962**, *1*, 111–122. [[CrossRef](#)]